Status Update of PSI Experiment R-89.01.1

A PRECISE MEASUREMENT OF THE $\pi^+ \to \pi^0 e^+ \nu$ DECAY RATE

THE PIBETA COLLABORATION

23 November 1995

The PIBETA project at PSI is a program of measurements with the aim of making a precise determination of the pion beta decay rate, initially to $\sim$ 0.5%. Significant delays as well as developments have occurred in this project since the original approval by the BV in 1992. The purpose of this document is to present a condensed update of the experimental method and the associated systematics.

1. Experimental Method

The experimental signature of a $\pi^+ \to \pi^0 e^+ \nu$ event is determined by the prompt decay $\pi^0 \to \gamma\gamma$. The small branching ratio ($\simeq 1 \times 10^{-8}$) for the $\pi\beta$ decay and the required high measurement precision impose stringent requirements on the experimental apparatus. The detector must be able to handle high event rates and cover a large solid angle with high efficiency for π^0 detection. Efficient hardware suppression of background events calls for good energy and timing resolution. At the same time the system must operate with low systematic errors and be subject to accurate calibration.

The Detector

We have chosen to detect decays at rest, and to use $\pi \to e\nu$ decays for normalization. Consequently, our apparatus has the following main components:

(i) beam counters and a segmented active target to stop the pions,

(ii) two concentric cylindrical multi-wire proportional chambers for charged particle tracking surrounding the active target,

(iii) a segmented fast veto counter surrounding the MWPCs,

(iv) a high resolution segmented fast shower calorimeter surrounding the active target and tracking detectors in a near-spherical geometry, and

(v) cosmic ray veto counters around the entire apparatus.

A schematic layout of the experimental apparatus is shown in Figs. 1 and 2.

The spatial, energy and time resolution of the segmented shower calorimeter are essential for efficient running at high rates. The PIBETA calorimeter geometry calls for 240 truncated

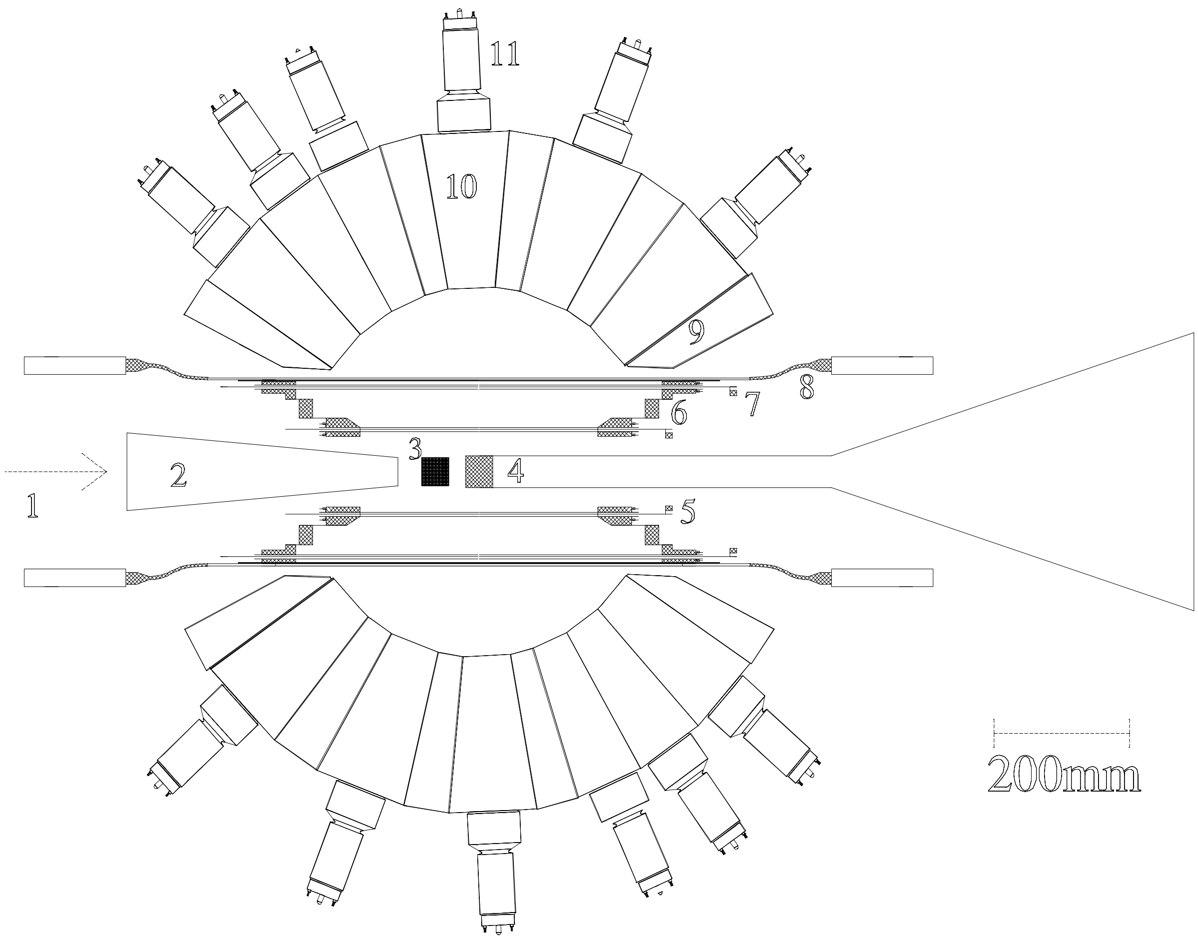

Fig. 1.(above) Schematic cross section of the PIBETA apparatus showing the main components: beam entry (1,2), active degrader (3), active target (4), MWPC's and support (5–7), plastic veto detectors and PMT's (8), pure CsI calorimeter and PMT's (9–11).

Fig. 2.(right) A view showing the geometry of the pure CsI shower calorimeter. The sphere is made up of 240 elements, truncated hexagonal, pentagonal, and trapezoidal pyramids; it covers about 80% of 4π in solid angle.

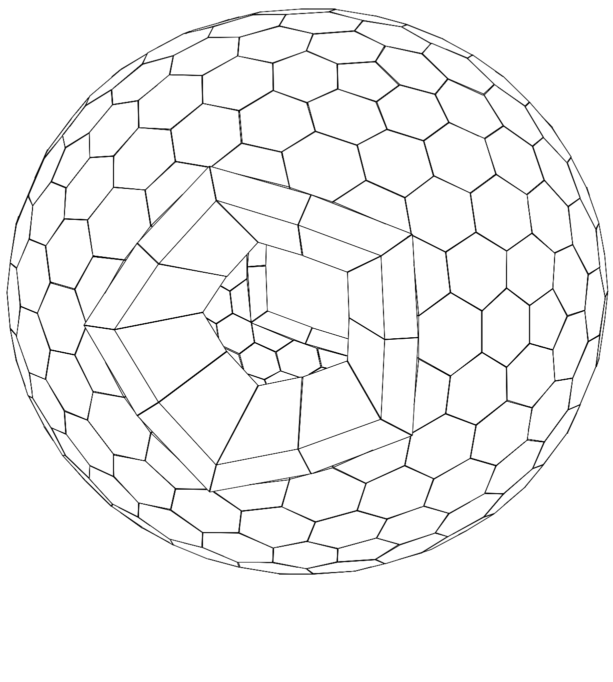

hexagonal and pentagonal pyramids; the shapes were chosen for optimum light collection efficiency, and the granularity to accommodate pion stop rates well in excess of 10^6 s^{-1}. The calorimeter modules are made of pure CsI (for speed) and are 22 cm thick, which is equivalent to 12 radiation lengths. The outer radius of the sphere is 48 cm. Efficient tracking of charged particles with good double track resolution is necessary for a clean identification of the $\pi \rightarrow e\nu$ decay events – hence the central tracking detectors.

The Triggers

Selective bias-free triggers capable of handling high rates are an essential requirement. We have designed fast analog hardware triggers optimized to accept nearly all non-prompt $\pi\beta$ and $\pi \rightarrow e\nu$ events contained in the calorimeter with individual shower energy exceeding the Michel endpoint (high threshold, HT $\simeq$ 55 MeV), while keeping the accidental rate to an acceptable level.

Each pion stopping in the target initiates a delayed pion gate (DPG) not longer than 100 ns, delayed by about 10 ns in order to avoid inclusion of prompt background events. Also generated are: (a) a short gate (PROMPT) coincident with the pion stop pulse, (b) a second delayed pion gate (DPG2) of the same duration as DPG but started 100 ns later, (c) a short gate (COSM) coincident with a cosmic muon passing through the veto housing, and a wide unbiased gate (NOBG) overlapping the pion stop time. Event triggers are generated on the basis of a coincidence of one of these gates and shower signal(s) in the calorimeter. Gates other than the DPG are necessary for a complete understanding of the background processes and for the calorimeter gain monitoring and stabilization.

Pion beta decays are registered during the DPG through a coincident detection of two γ rays (from $\pi^0 \rightarrow \gamma\gamma$) in the shower calorimeter. The two photons are emitted nearly back-to-back with about 67 MeV each. The positron is detected in the active target but will not be included in the trigger, to avoid biasing it. The trigger requires two localized showers occurring in opposing hemispheres of the calorimeter, each exceeding the HT. In addition, there is a low-threshold version (LT $\simeq$ 2 MeV) of the same trigger for background study purposes. Both the high- and low-threshold $\pi\beta$ triggers are replicated in the late DPG2 gate. The low-threshold triggers are appropriately prescaled.

$\pi \rightarrow e\nu$ decays are identified by means of a dedicated trigger requiring a localized single shower during the DPG with energy deposited in the calorimeter exceeding HT. Due to the much higher branching ratio, the $\pi \rightarrow e\nu$ triggers are prescaled. As for the $\pi\beta$ trigger, low- and high-threshold versions of the trigger are implemented during both the DPG and the late DPG2 gates, all suitably prescaled.

A good $\pi\beta$ or $e\nu$ event is not allowed to be followed closely by a beam particle in order to avoid pileup caused by a prompt event.

The proper working of the trigger relies on fast analog summing and discrimination of the CsI module signals and an appropriate shower clustering scheme. The size of the CsI crystal modules was chosen to match approximately the characteristic lateral spreading of such showers, so that a typical shower deposits most of its energy in three crystals sharing a common vertex point. Hence, we sum over each of the vertices of the active calorimeter, using overlapping summing regions for maximum trigger efficiency. Analog summing and discrimination is performed in dedicated linear summer/discriminator modules (UVA-125).

The basic energy summing regions, called clusters, sum over 9 detector modules each, which is consistent with the planned pion stop rates below 10^7 s^{-1}. Because clusters have to overlap, an individual crystal contributes energy to up to three clusters using linear splitters (UVA-126). There are 60 clusters in the entire calorimeter.

In order to simplify the trigger logic, the calorimeter is divided into 10 main regions called superclusters, each made up of a logical OR of 6 overlapping clusters centered about a pentagonal shaped detector. Each of the 10 superclusters has an associated opposing hemisphere (complement) made up of the logical OR of the 5 superclusters not neighboring it (cf. Fig. 3). Thus, for example, a $\pi\beta$ trigger would require a coincidence of a given supercluster with its complement inside the DPG gate.

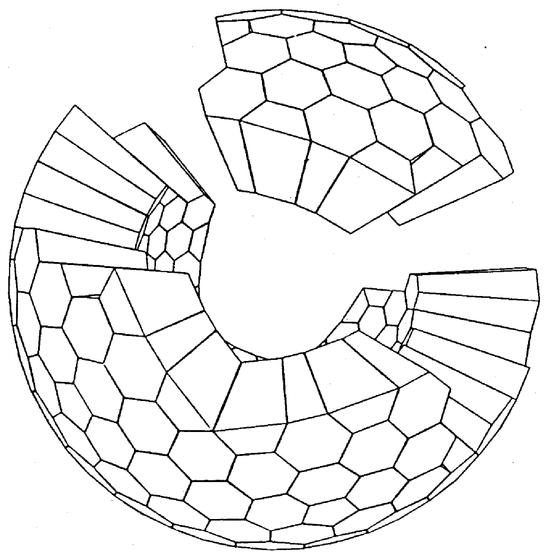

Fig. 3. One supercluster and its complement.

The analog energy summing method has been successfully tested in a $\pi\to e\nu$ test measurement using a partial setup consisting of 26 CsI modules. Six overlapping clusters were defined with up to 9 detectors each, and a supercluster logical OR was formed. As described above, $e\nu$-LT and $e\nu$-HT triggers were formed. A resulting energy spectrum is shown in Fig. 4.

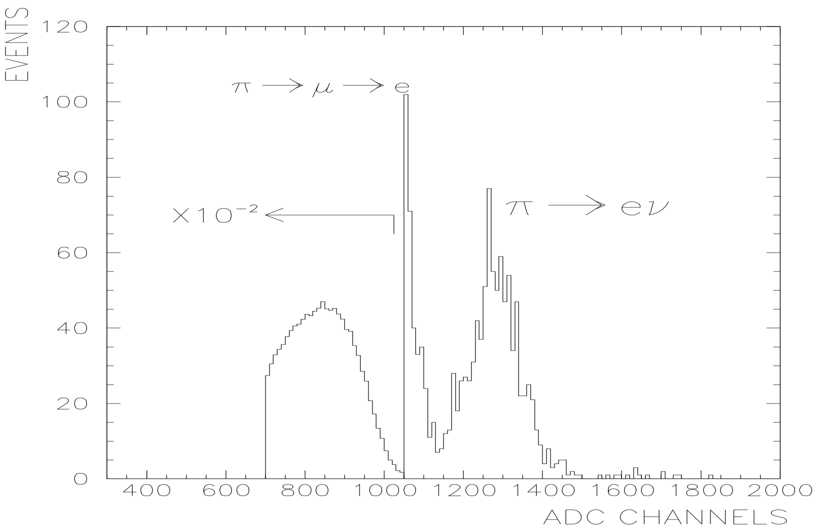

Fig. 4. $\pi\to e\nu$ events and background recorded in a 26-detector CsI array viewing a stopped pion target. The low energy portion of the Michel spectrum is suppressed by a factor of 100. The energy scale is 20 channels/MeV. The dip between the Michel endpoint and the $\pi\to e\nu$ peak at 55 MeV is in good agreement with our GEANT results.

Instrumental Improvements

A significant new addition to the experiment is due to the recent development by our PSI collaborators Ch. Brönnimann, R. Horisberger and R. Schnyder of a fast (up to 800 MHz) inexpensive "domino" sampling chip (DSC) to be used in conjunction with each calorimeter phototube. All calorimeter and active target signals will be digitized. Using the digitizer will help us achieve higher background pileup suppression and, thus, improved calorimeter energy resolution at higher event rates. No less important will be the improvement of the timing resolution due to the sampling. Current estimates indicate that sub-100 ps rms accuracy in determining the relative time of the leading edge of digitized CsI pulses should be attainable. The final accuracy of the method will depend on the noise level in the actual signal pulse shapes.

We had originally considered such a device for a more advanced stage of the experiment. However, successful initial tests have made the chip available sooner. Currently a dedicated PIBETA circuit board with zero suppression and appropriate readout features is under development at PSI. The device is about one to two years away from being fully integrated into the PIBETA apparatus and routinely operational.

2. Backgrounds and Their Suppression

Background processes to be distinguished from $\pi\beta$ and $e\nu$ events fall into two groups: (a) prompt events due to the strong interactions of the beam pions with any matter in their path, and (b) delayed events due to other weak processes, i.e., π and μ decays. Particularly important prompt background processes are pion capture reactions followed by neutron and/or gamma emission. Among the delayed background processes are the following decays (branching ratios in parentheses):

$$\begin{array}{lllllll} \pi^+ & \rightarrow & \mu^+\nu(\gamma) & (1.0), & \text{and} \quad \mu^+ & \rightarrow & \mathrm{e}^+\nu\overline{\nu}(\gamma) \quad (1.0), \\ & & \mathrm{e}^+\nu(\gamma) & (\sim 1.2\times10^{-4}), & & & \mathrm{e}^+\nu\overline{\nu}\mathrm{e}^+\mathrm{e}^- \quad (\sim 3\times10^{-5}), \\ & & \mathrm{e}^+\nu e^+e^- & (\sim 3\times10^{-9}), & & & \end{array}$$

as well as their accidental coincidences.

Backgrounds from Beam Hadronic Interactions

Suppression of prompt backgrounds is necessary for obtaining clean spectra of both $\pi\beta$ and $\pi\rightarrow e\nu$ events. Hadronic interactions of the beam pions in the active degrader (AD) and active target (AT) involve scattering, charge exchange and nuclear reactions. All have been studied in detail in our GEANT simulations. Main results of that analysis are discussed in a separate "PIBETA Note" accessible at the PIBETA home page.[1] We summarize here the essential points.

Hadronic scattering of pions in AT and AD leads to the same final outcome as Coulomb scattering, namely, a delayed decay of the stopped pion.

Pion single charge exchange (SCX) in the AD and AT is the exclusive source of hard prompt neutral showers with the branching ratio of about 1×10^{-6} folded with our acceptance. Because they are prompt and are vetoed efficiently by the delayed trigger gate, these events present a problem only when they occur during an already open gate by virtue of an undetected second beam pion charge exchanging in our beam detectors. A suppression factor of 10^{-6} is required in order to bring this background down to the level of 0.1% of the $\pi\beta$ rate. This is easily achieved by the beam counters B1 and AD, both of which are small efficient plastic scintillators with optimized light readout. In addition, the probability for a second beam pion is only 0.02 per beam bucket at the beam rate of 10^6 s^{-1}.

Charged ejectiles following pion hadronic interactions in the AD and AT occur with the branching ratio of $\sim 0.96\%$ and deposit up to about 100 MeV in the calorimeter. Absence of a high-energy continuum background characteristic for the prompt events in Fig. 4 shows that we have been able to suppress it very well already in our test runs without having the benefit of the full complement of charged particle tracking detectors.

Backgrounds from Muon and Pion Decays

Since ours is a stopped experiment, the overwhelming source of background are the muon decay events. The main triggers, $\pi\beta$ and $\pi\to e\nu$, both rely on discrimination (HT) to suppress single Michel events. Thus, the main impact of muon decays on our measurements is through accidental coincidences. The CsI spectra resulting from the relevant processes are shown in Figs. 5–8 for the $\pi\beta$ and $\pi\to e\nu$ triggers, respectively. The rates and suppression factors are listed below, in Tables 1 and 2 for the range of pion stop rates of interest.

Of the pion decays, the radiative decay $\pi\to e\nu\gamma$ is the only one with serious consequences for our data sample and systematics. On the other hand, that problem is alleviated by the fact that the PIBETA detector is highly suitable for the study of this decay. As shown in Figs. 5 and 6, these events are well suppressed by off-line software cuts on colinearity and charge particle counters.

The more significant effect of the $\pi\to e\nu\gamma$ events is on our normalization. At our current level of Monte Carlo simulation we find that our acceptance for the $\pi\to e\nu\gamma$ decay is approximately 98.9% of a hypothetical pure $\pi\to e\nu$ decay, making it a 1.1% correction. (The measured branching ratio for the $\pi\to e\nu$ decay, to be used in our normalization, includes the radiative decay.) We are further refining our modeling of this decay, but are confident that we can produce a better than 10% uncertainty on this correction from both simulation and direct measurement.

Summary of Rates and Suppression Factors

Since non-radiative decays are unphysical and do not occur in nature, we have included the full treatment of the radiative decays of the pion and muon in our Monte Carlo simulations. Neither in figures nor in the summary tables below do we make the artificial separation of the nonradiative decays. The results presented in the Tables 1 and 2 below are to be taken as work in progress, as we are continually improving our GEANT codes.

We present results of calculations at two beam stopping rates which bracket our nominal running rate of 10^6 s^{-1}. The "Branching Ratios" column in the tables lists the physical branching ratios for the single decay event types. In the case of accidental coincidences of several decays, the "branching ratios" give the probability of that occurrence given the stopping rate and the coincidence gate width.

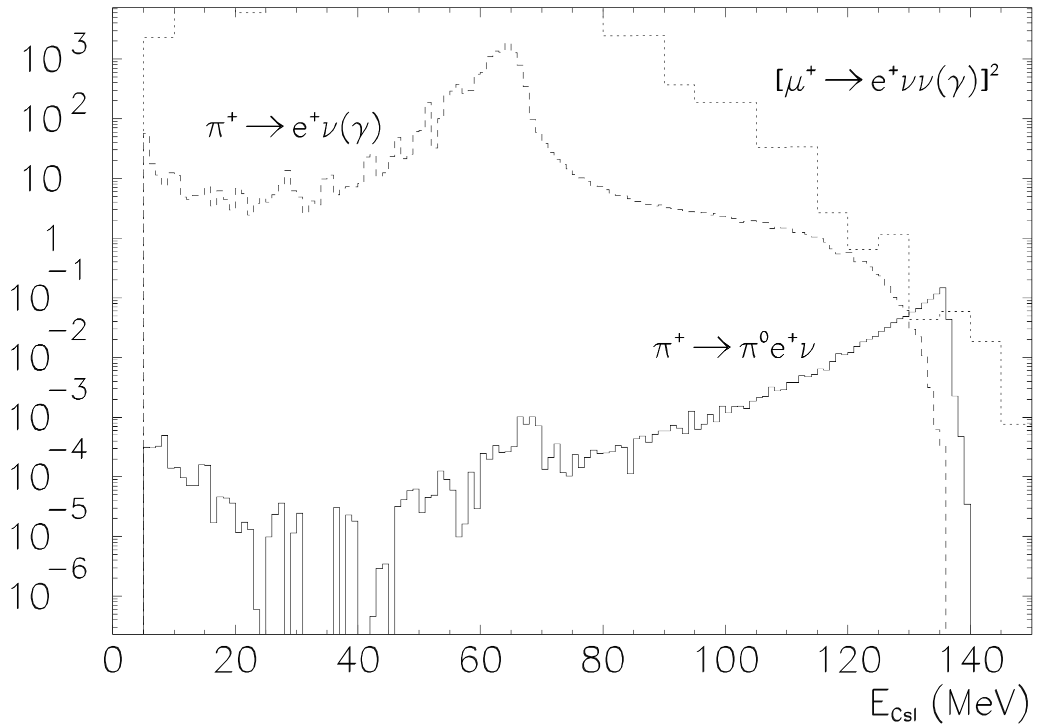

Fig. 5. Spectrum of energies deposited in the calorimeter by background events due to muon and pion decays as registered by the $\pi\beta$-LT trigger (GEANT simulation).

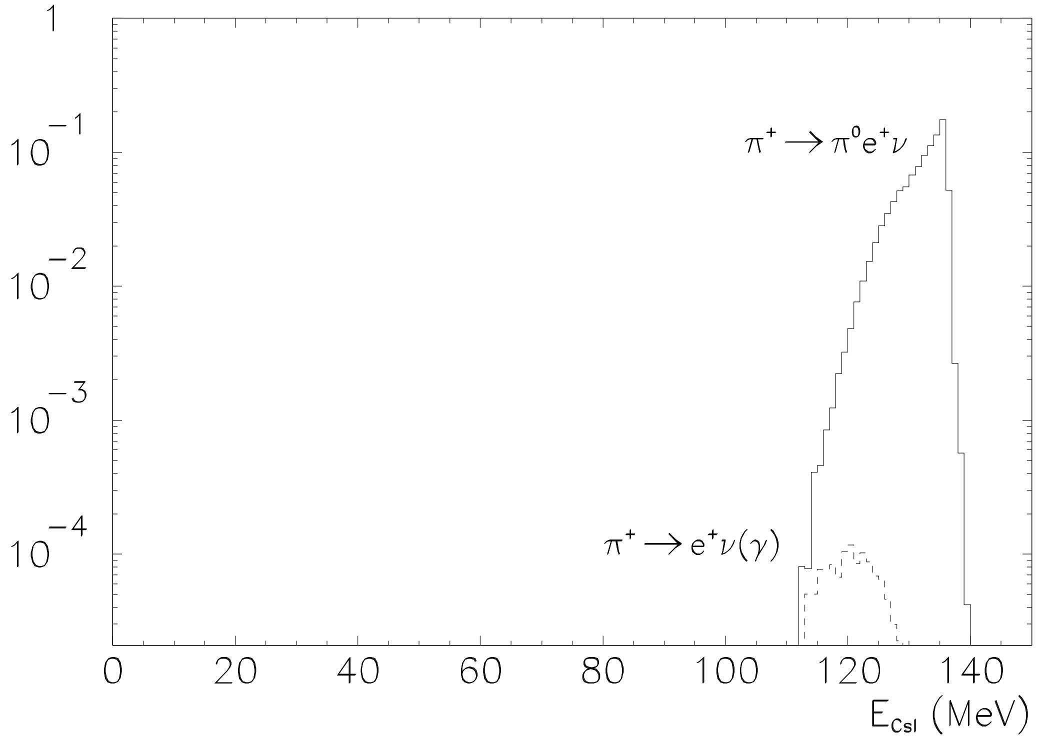

Fig. 6. Spectrum of energies deposited in the calorimeter by background events due to muon and pion decays in the $\pi\beta$-HT trigger, after software cuts (GEANT simulation).

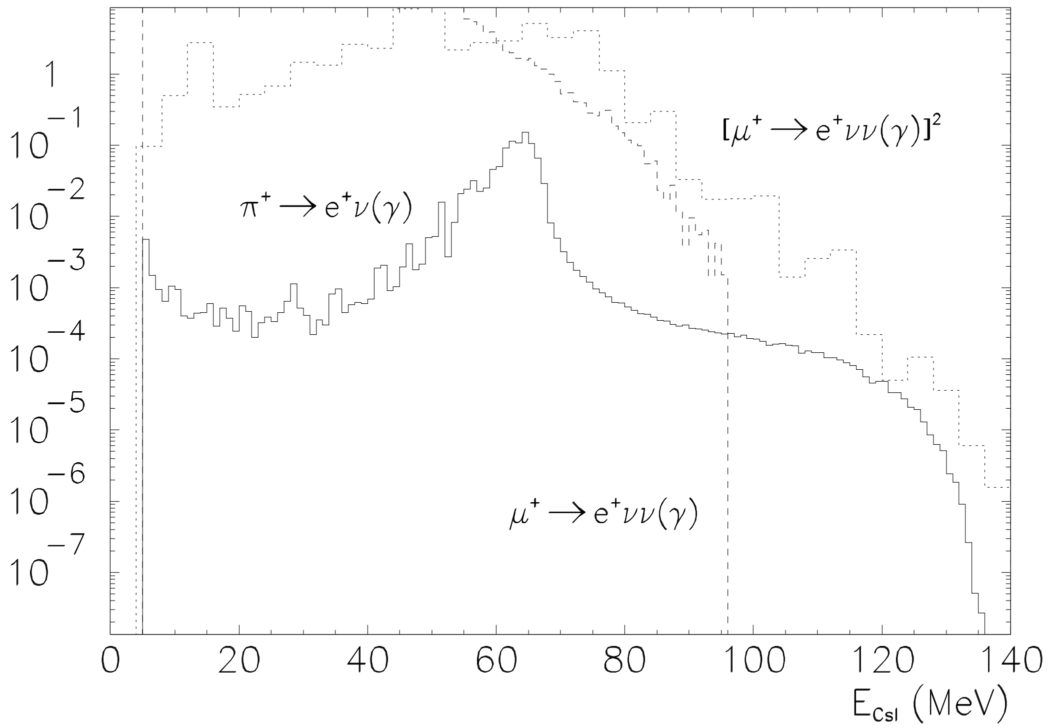

Fig. 7. Spectrum of energies deposited in the calorimeter by background events due to muon and pion decays registered in the $e\nu$-LT trigger (GEANT simulation).

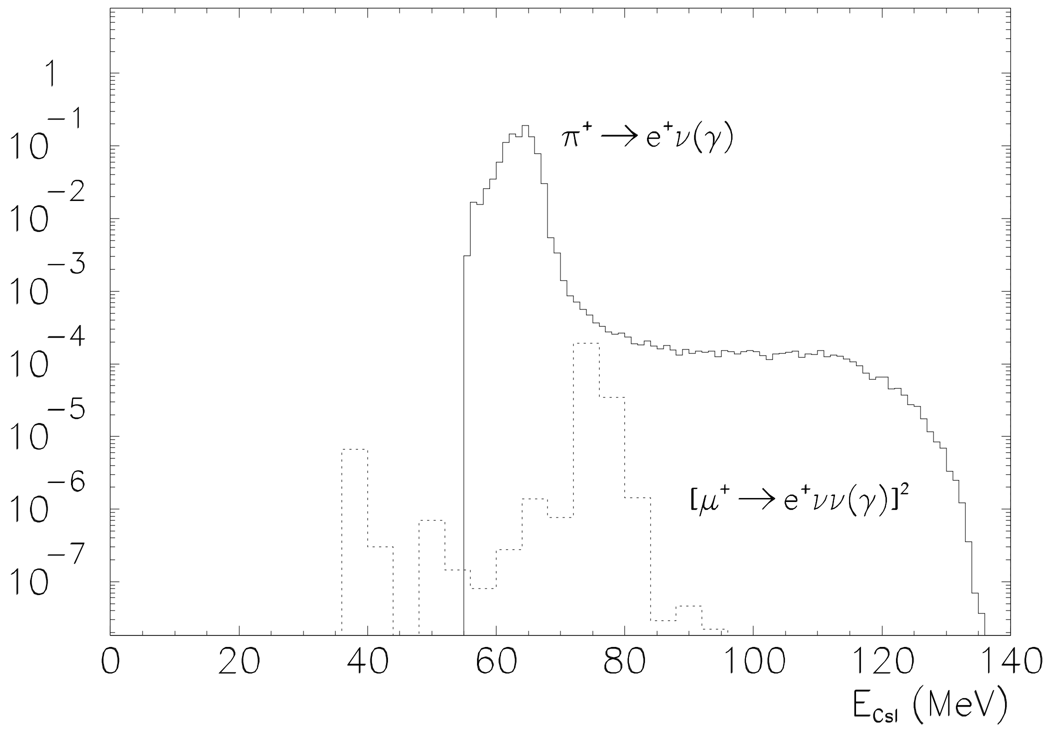

Fig. 8. Spectrum of energies deposited in the calorimeter by background events due to muon and pion decays in the $e\nu$-HT trigger, after software cuts (GEANT simulation).

Table 1. Main trigger and background rates at the beam stop rate of 5×10^5 s^{-1} (GEANT simulation).

Reaction	"Branching Ratio"	Integrated Acceptance	Prescale Factor	Trigger Rate (s^{-1})	Software Suppression
		$\pi^+ \to \pi^0 e^+ \nu$ trigger			
$\pi^+ \to \pi^0 e^+ \nu$	$1.0 \cdot 10^{-8}$	0.637 ± 0.003	1	$2.1 \cdot 10^{-3}$	1
$\pi^+ \to e^+ \nu(\gamma)$	$1.2 \cdot 10^{-4}$	$(2.09 \pm 0.04) \cdot 10^{-5}$	1	$8.4 \cdot 10^{-4}$	$5 \cdot 10^{-6}$
$[\mu^+ \to e^+ \nu\nu(\gamma)]^2$	$9.9 \cdot 10^{-3}$	$(1.8 \pm 0.6) \cdot 10^{-9}$	1	$9.0 \cdot 10^{-6}$	$5 \cdot 10^{-12}$
$[\mu^+ \to e^+ \nu\nu(\gamma)]^3$	$9.9 \cdot 10^{-5}$	$\leq 3 \cdot 10^{-8}$	1	$\leq 1.5 \cdot 10^{-6}$	$\leq 10^{-15}$
$[\mu^+ \to e^+ \nu\nu(\gamma)]^4$	$9.9 \cdot 10^{-7}$	$\leq 3 \cdot 10^{-7}$	1	$\leq 1.5 \cdot 10^{-7}$	$\leq 10^{-20}$
$[\mu^+ \to e^+ \nu\nu(\gamma)]$ $\times[\pi^+ \to e^+ \nu(\gamma)]$	$1.2 \cdot 10^{-6}$	$(1.6 \pm 0.1) \cdot 10^{-4}$	1	$6.2 \cdot 10^{-5}$	10^{-12}
		$\pi^+ \to e^+ \nu$ trigger			
$\pi^+ \to e^+ \nu(\gamma)$	$1.23 \cdot 10^{-4}$	0.667 ± 0.003	10^2	0.27	1
$[\mu^+ \to e^+ \nu\nu(\gamma)]^2$	$9.9 \cdot 10^{-3}$	$(1.5 \pm 0.1) \cdot 10^{-2}$	10^2	0.76	$5 \cdot 10^{-6}$
$[\mu^+ \to e^+ \nu\nu(\gamma)]^3$	$9.9 \cdot 10^{-5}$	$(3.1 \pm 0.1) \cdot 10^{-2}$	10^2	$1.5 \cdot 10^{-2}$	$1.6 \cdot 10^{-10}$
$[\mu^+ \to e^+ \nu\nu(\gamma)]^4$	$9.9 \cdot 10^{-7}$	$(4.4 \pm 0.2) \cdot 10^{-2}$	10^2	$2.2 \cdot 10^{-2}$	$1.6 \cdot 10^{-10}$

Table 2. Main trigger and background rates at the beam stop rate of 2×10^6 s^{-1} (GEANT simulation).

Reaction	"Branching Ratio"	Integrated Acceptance	Prescale Factor	Trigger Rate (s^{-1})	Software Suppression
		$\pi^+ \to \pi^0 e^+ \nu$ trigger			
$\pi^+ \to \pi^0 e^+ \nu$	$1.0 \cdot 10^{-8}$	0.637 ± 0.003	1	$7.6 \cdot 10^{-3}$	1
$\pi^+ \to e^+ \nu(\gamma)$	$1.2 \cdot 10^{-4}$	$(2.09 \pm 0.04) \cdot 10^{-5}$	1	$3.1 \cdot 10^{-3}$	$5 \cdot 10^{-6}$
$[\mu^+ \to e^+ \nu\nu(\gamma)]^2$	$3.8 \cdot 10^{-2}$	$(1.8 \pm 0.6) \cdot 10^{-9}$	1	$1.4 \cdot 10^{-4}$	$5 \cdot 10^{-12}$
$[\mu^+ \to e^+ \nu\nu(\gamma)]^3$	$1.5 \cdot 10^{-3}$	$\leq 3 \cdot 10^{-8}$	1	$\leq 9.0 \cdot 10^{-5}$	$\leq 10^{-15}$
$[\mu^+ \to e^+ \nu\nu(\gamma)]^4$	$6.1 \cdot 10^{-5}$	$\leq 3 \cdot 10^{-7}$	1	$\leq 3.6 \cdot 10^{-5}$	$\leq 10^{-20}$
$[\mu^+ \to e^+ \nu\nu(\gamma)]$ $\times[\pi^+ \to e^+ \nu(\gamma)]$	$4.7 \cdot 10^{-6}$	$(1.6 \pm 0.1) \cdot 10^{-4}$	1	$9.6 \cdot 10^{-4}$	10^{-12}
		$\pi^+ \to e^+ \nu$ trigger			
$\pi^+ \to e^+ \nu(\gamma)$	$1.2 \cdot 10^{-4}$	0.667 ± 0.003	10^2	1.0	1
$[\mu^+ \to e^+ \nu\nu(\gamma)]^2$	$3.8 \cdot 10^{-2}$	$(1.5 \pm 0.1) \cdot 10^{-2}$	10^2	11.6	$5 \cdot 10^{-6}$
$[\mu^+ \to e^+ \nu\nu(\gamma)]^3$	$1.5 \cdot 10^{-3}$	$(3.1 \pm 0.1) \cdot 10^{-2}$	10^2	0.92	$1.6 \cdot 10^{-10}$
$[\mu^+ \to e^+ \nu\nu(\gamma)]^4$	$6.1 \cdot 10^{-5}$	$(4.4 \pm 0.2) \cdot 10^{-2}$	10^2	$5.4 \cdot 10^{-2}$	$1.6 \cdot 10^{-10}$

3. Measurement Uncertainties

The $\pi\beta$ decay rate is evaluated from the ratio:

$$\frac{1}{\tau_{\pi\beta}} = \frac{1}{\tau_\pi} \cdot BR_{\pi\beta} = \frac{BR_{e\nu} f_{\rm presc}}{\tau_\pi + BR_{\pi\to\gamma\gamma}} \cdot \frac{A_{e\nu}}{A_{\pi\beta}} \cdot \frac{N_{\pi\beta}}{N_{e\nu}} \quad , \tag{1}$$

where τ_π is the pion lifetime, $N_{\pi\beta}$ and $N_{e\nu}$ represent the numbers of good $\pi\beta$ and $\pi\to e\nu$ events, respectively, $A_{\pi\beta}$ and $A_{e\nu}$ are the detector acceptances for the $\pi\beta$ and $\pi\to e\nu$ events, respectively, while $f_{\rm presc}$ is the the prescale factor for the $\pi\to e\nu$ trigger.

Due to the similarities between the two classes of events, the acceptances $A_{\pi\beta}$ and $A_{e\nu}$ are nearly equal. At the same time both are functions of many parameters:

- (a) geometrical solid angle covered by the calorimeter including the effects of:
  - (i) lateral and axial extent of the pion stopping distribution,
  - (ii) cracks between the CsI detector modules,
  - (iii) alignment uncertainties;
- (b) lineshapes of the calorimeter detector modules' response to photon- and positron-induced showers; details of the lineshapes are affected by:
  - (i) electromagnetic shower processes in CsI: leak-through, lateral spreading, back-splash,
  - (ii) electromagnetic interactions in the active target and tracking detectors: bremsstrahlung, Bhabha scattering and in-flight annihilation for the positrons, pair production, Compton scattering, etc. for photons,
  - (iii) volume uniformity of the CsI detector light response and photoelectron statistics,
  - (iv) gain stability of the calorimeter detector modules, and
  - (v) photonuclear and electron knockout reactions in CsI.

In addition, efficiencies of the charged particle detectors used in the software cuts to remove the Michel and hadronic backgrounds from the final data sample also affect the overall uncertainty.

We are continuing the study of these processes with increasing precision. The important processes will be measured on-line and/or in dedicated calibration runs, as well as simulated. A few less significant processes can be reliably simulated with accuracy sufficient for our purposes. For illustration, we show the GEANT simulated acceptances $A_{\pi\beta}$ and $A_{e\nu}$ in Fig. 9 as functions of the cosine of the shower-reconstructed polar angle θ.

Integrated Absolute Acceptances

The shapes of the differential acceptance functions $A(\theta)$ will, of course, be precisely measured on-line in our experiment. However, absolute normalization of these functions is necessary in order to obtain the absolute integral acceptances appearing in Eq. (1). To this end we will perform independent high-statistics measurements of the same quantities in well

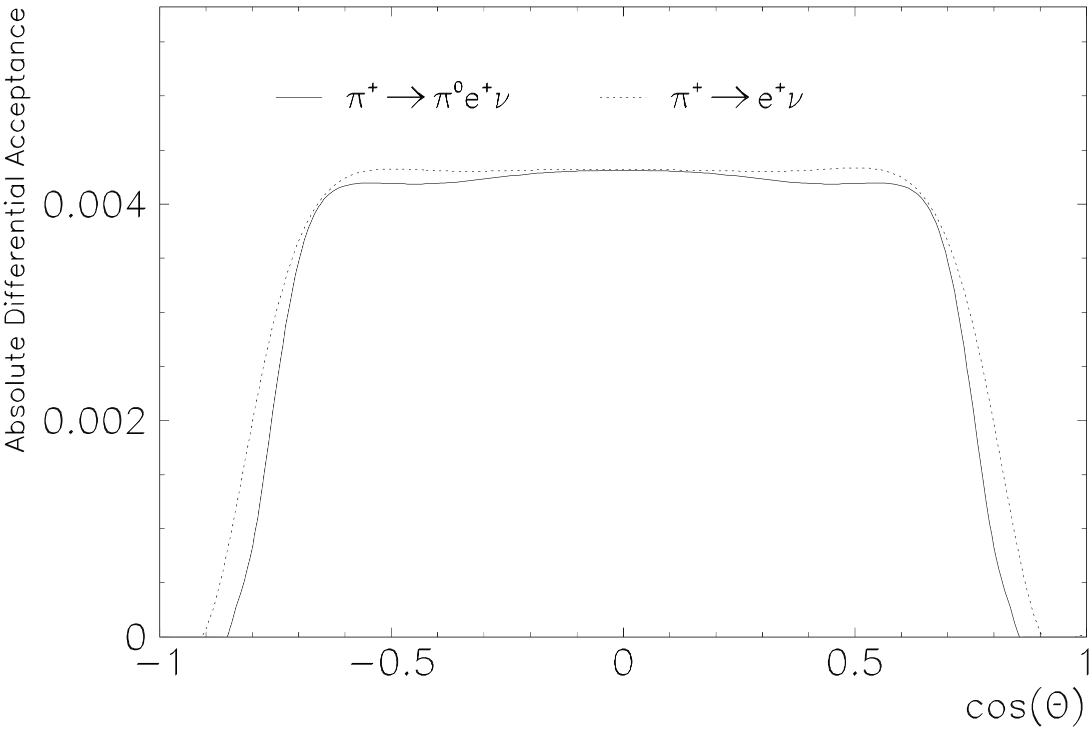

Fig. 9. GEANT calculated absolute differential acceptance of our apparatus for $\pi\beta$ and $\pi \to e\nu$ events as a function of $\cos\theta$. This work is in progress and minor corrections will occur as the PIBETA GEANT code is being made more realistic.

controlled setups. Differential acceptance will be measured along strips of constant azimuthal angle ϕ over the significant range of θ in a section of the sphere using tagged positrons and photons. Absolute measurements of $A(\theta)$ between $\theta = 0$ and $90°$ for single positrons and photons with about 5×10^6 events each are required to determine the ratio of the absolute integrated acceptances $A_{\pi\beta}/A_{e\nu}$ with an uncertainty of $\sim$ 0.2–0.3% when combined with other corrections. Here is how we plan to make the measurements.

Positron Response We will tune the PSI πE1 beamline for 70 MeV/c positrons, producing a low-intensity defocused beam on the face of the CsI crystals. The positrons will be momentum-analyzed and additionally identified by their time of flight with respect to the 50 MHz accelerator RF pulse. Positron trajectories will be tracked by means of thin wire chamber detectors. In this way we can illuminate evenly a large section of the CsI calorimeter at once and obtain relatively quickly a detailed position-dependent event-by-event calorimeter response. One result of a test run without beam momentum analysis is shown in Fig. 10, and compares favorably with GEANT simulation.

Our simulation of in-flight annihilations and scattering will be calibrated by inserting plastic scintillator material of variable thickness in the positron beam in front of the CsI. A thin plastic scintillation counter will be used to determine the number of falsely neutral showers. These measurements will be carried out with high statistics in order to enable stringent off-line cuts and clean data samples.

The same set of measurements will be repeated for lower positron momenta in order to

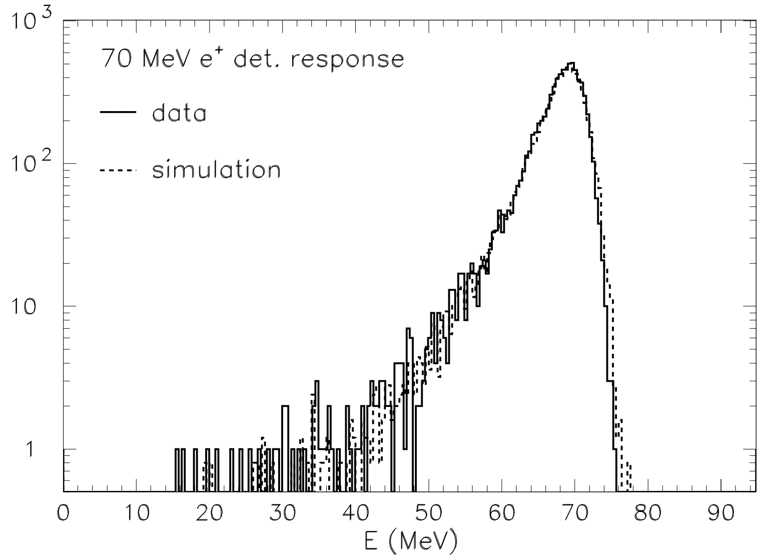

Fig. 10. Spectrum of energy deposited in a 26-module section of the calorimeter by 70 MeV/c positrons, and GEANT simulation. The simulation includes effects of photoelectron statistics and light nonuniformity.

calibrate the calorimeter response for the Michel positrons.

Gamma Response An analogous program of measurements will be carried out with photon-induced showers. For this purpose, we shall use a stopped π^- beam in a liquid hydrogen target, using the reaction $\pi^- p \to \pi^0 n$. The π^0's in the above reaction carry some 2.9 MeV of kinetic energy, which results in a total energy range for the two decay photons of $\sim 54 - 83$ MeV. This range includes all of the photon energies of interest for the pion beta decay measurement (65.6 – 69.4 MeV). A desired photon energy from the above range can be selected by appropriately positioning the neutron detector with respect to the shower counter and using suitably positioned second photon "tag" counters. This method allows for a simultaneous mapping of several positions on the shower counter with desired photon energies. A simplified schematic layout of the detector arrangement is shown in Fig. 11. Preliminary results of a test run with a 26-counter CsI array using the detector arrangement of Fig. 11 are shown in Fig. 12.

As in the case of the positron response, we need to measure the effects of the active target, tracking detectors and air on the photon acceptance (pair creation, Compton scattering, photonuclear reactions, etc.) Again, we will insert plastic scintillator material of variable thickness in front of the CsI. Throughout the measurements, a thin plastic veto counter will register the charged component of the shower backsplash producing false vetos. The effects of the active target and tracking counters are of the order of 1 – 2% for both $A_{\pi\beta}$ and $A_{e\nu}$. The planned counting statistics of over 10^6 will ensure error bars in the range of a few percent, i.e., well under 0.1% on the acceptances.

We note that both the photon and positron calibration data will reflect the full extent of the photonuclear processes in CsI induced by electromagnetic showers. Also folded in the same data will be the effects of photoelectron statistics, nonuniformity of the detector light response, and cracks. The CsI array to be calibrated will comprise about 1/4 of the sphere. Deviations in the differential acceptance functions across the remaining 3/4 of the sphere will be determined from (a) the on-line $\pi \to e\nu$ data for the positrons where counting statistics is not a limiting factor, and (b) a repeated calibration measurement of the $\pi^- p \to \pi^0 n$ reaction with a hydrogen target inside the sphere.

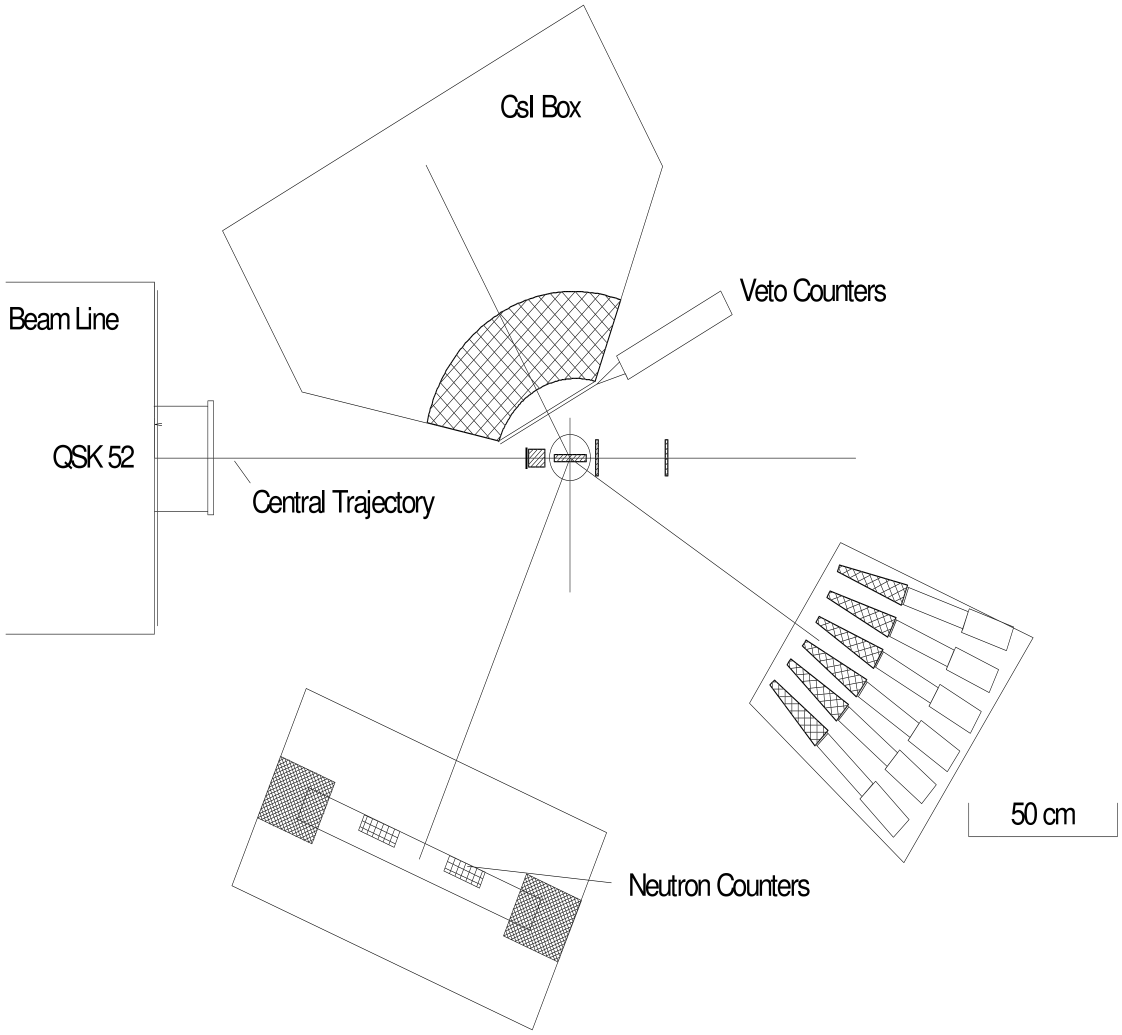

Fig. 11. A schematic detector layout for the calibration of the CsI calorimeter response to photons.

However, we wish to understand and simulate our acceptance functions in detail, as a check that we have all above elements of the systematics under control. To that end we have included in our GEANT code the effects of the photonuclear reactions, photoelectron statistics, detector light response nonuniformity and cracks, and are currently refining our treatment of each of these effects.

Photonuclear reactions are added to GEANT on the basis of the published compilations of cross sections[2]. The total probability for a $\pi\beta$ photon to undergo a photonuclear interaction outside the CsI calorimeter is $0.033 \pm 0.011\%$, while the total probability of a photonuclear interaction during a shower inside CsI is $0.33 \pm 0.12\%$. However, the effect on the tail cutoff is further reduced, and there are additional cancellations in the acceptance ratio $A_{e\nu}/A_{\pi\beta}$. Details of the effect of photonuclear processes on the CsI lineshapes are presently being refined.

Our routine procedure for the acceptance or rejection of each CsI detector module involves three concurrent measurements in a dedicated calibration facility specifically set up for that

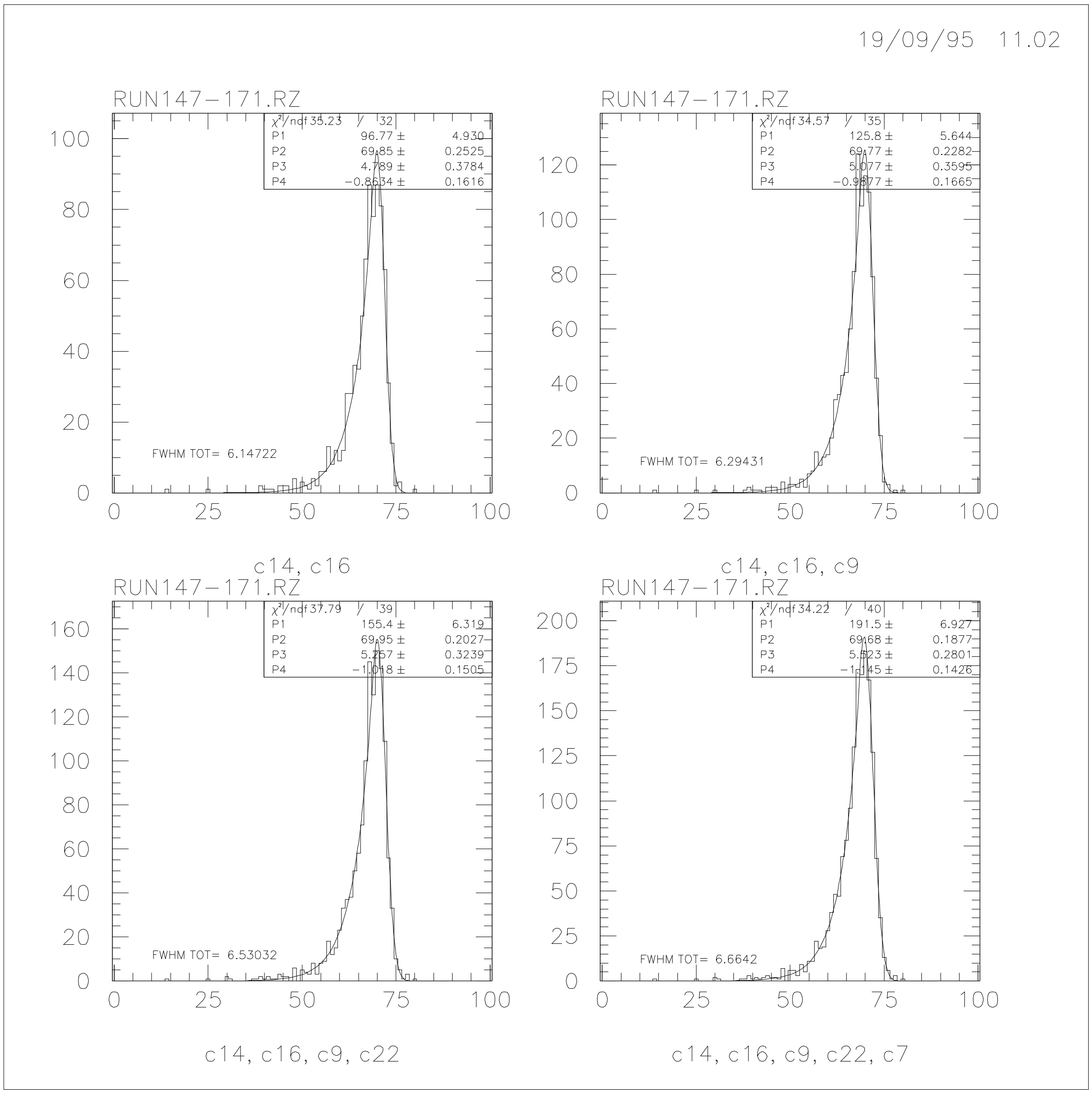

Fig. 12. CsI detector response to photons for several groups of detectors out of an array of 26 counters, measured using the reaction $\pi^- p \rightarrow \pi^0 n$ (preliminary).

purpose at PSI. The quantities measured are: (i) the average number of photoelectrons/MeV, (ii) the optical uniformity of the module's light response through a detailed cosmic muon tomography of the detector volume, and (iii) the ratio of fast to the total light output for minimum ionization particles. The complete detector database will ensure an unambiguous folding of the detector response parameters with the electromagnetic shower response.

Dynamic Gain Stabilization

Since our absolute acceptances involve an energy cutoff, properly stabilized gains are crucial for keeping the uncertainties low. Besides the usual sources of gain instability in the electronics and phototubes, CsI itself has a pronounced temperature coefficient of light output of about $-1.5\%/^\circ$C. Given the drifts in ambient temperature in the experimental hall, this would result in unacceptable shifts. Therefore the entire detector system will be housed in a temperature stabilized enclosure with temperature drifts regulated within 0.5°C.

The overall gain of the system will be dynamically monitored and stabilized by taking Michel events in the calorimeter with a rate of up to 200 Hz during the entire experiment. The Michel spectrum of the muon decay falls off rapidly around 50 MeV, producing a distinctive edge in each detector very suitable for use in gain calibration. Using realistic spectra from test runs we find for the uncertainty of the Michel edge position:

$$\Delta E = 17.9 \times \frac{1}{\sqrt{N}} \text{ (MeV)} \quad ,$$

where N is the number of events in the Michel spectrum between 5 MeV and 50 MeV. To achieve, e.g., a gain calibration accuracy of 0.5 MeV at 50 MeV (1%), a total of 1300 events are necessary. With the planned data acquisition rate this can be done in about 10 seconds for the whole detector. In other words, we can compensate a common gain drift of all channels over very short time intervals. It takes about 50 minutes to acquire the necessary statistics per channel in order to compensate the gain drift of individual detector modules. Therefore, this method is well suited for the individual PMT gain drifts which have time constants on the order of hours.

Our calorimeter detectors run at a very low rate, under 10^4 pulses per second. Nevertheless, after a careful study we have selected for use in the calorimeter photomultiplier tubes with CsSb dynodes that display a much higher degree of stability with respect to rate changes than the PMT's with the ordinary BeCu dynodes. In addition, the PMT bases have been designed for high linearity and gain stability vs. changes in load (see the PIBETA experiment home page for details[1]).

In summary, taking $e\nu$ lineshapes and software energy cutoffs from our test runs, we obtain an effect of 0.1% with a gain stabilization of 2.7%. We expect to do better than that without major difficulties.

We finally note that the gain stabilization system is being designed to operate fully automatically, without critical human intervention, in order to ensure long-term stability.

Geometrical Uncertainties

The main source of uncertainty of geometrical nature in the absolute acceptances $A_{e\nu}/A_{\pi\beta}$ has to do with the position and spatial spreading of the pion beam stopping distribution. Due to the cylindrical symmetry of our detector system the uncertainties can be broken down into the lateral and axial ones. Of the two, lateral uncertainties produce a larger effect on the acceptances than the axial. Also, since the $\pi\beta$ events require symmetrical coverage for the two photons emitted in the π^0 decay (nearly at rest), $A_{\pi\beta}$ is affected far more than $A_{e\nu}$. We discuss here the dominant sources of uncertainty.

The ratio $A_{e\nu}/A_{\pi\beta}$ is reduced by approximately 0.34% per 1 mm of lateral displacement of the center of the beam stopping distribution away from the central axis of the detector. This result was obtained using the realistic pion stopping distributions measured in our test runs.

Analogously, increasing the width of the lateral size of the pion stopping distribution by $\Delta\sigma = 1$ mm, where σ is the rms of the distribution in the lateral direction, changes $A_{e\nu}/A_{\pi\beta}$ by about 0.33%. For scale, we note that our measured pion stopping distribution has a lateral rms of about 5 mm.

Thus both the centroid and the width of the pion stopping distribution have to be monitored and controlled dynamically, as in the case of the gain of the CsI detectors. The regular active target is segmented into 9 regions, as shown in the GEANT drawing of the cross section of the central detector region in Fig. 13. Prompt signals from each of the target segments will be counted in a scaler, and the scalers read out every 10 s. The 5 central detectors receive practically the entire stopped beam, each counting at the same rate. The counting asymmetry (left–right or up–down) equals 2% for a shift of the centroid of 0.06 mm, corresponding to a 0.02% change in the integrated acceptance ratio. This is an easily measurable asymmetry given the counting statistics of 10^7 in 10 s, even after the Poisson corrections for unresolved double hits and accidental coincidences with Michel decays. Analysis of the measurement of the rms width of the distribution shows that a 2% central–peripheral asymmetry corresponds to a change in σ by 0.11 mm, or a 0.04% effect on the acceptance ratio $A_{e\nu}/A_{\pi\beta}$.

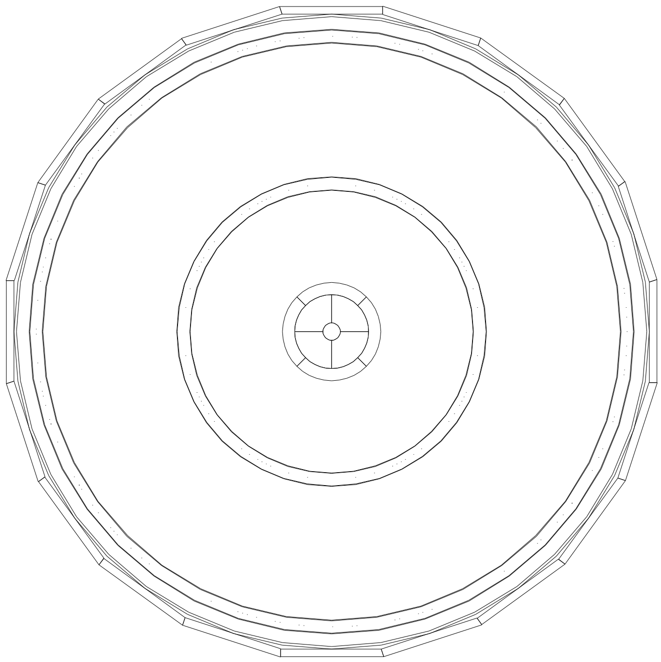

Fig. 13. Cross section of the PIBETA central detector region (drawn by GEANT). The beam axis is perpendicular to the page.

In addition, beam profiles will be monitored by active veto counters lining the beam pipe just upstream of the degrader/target area. These counters will not cut into the beam, but will detect the muon decay halo. Techniques of stabilizing the beam geometry using differential counting techniques have been implemented successfully by members of the PIBETA collaboration in past experiments.

Periodically we will insert our 79-element fiber active target into the apparatus in order to remeasure the shape of the stopping distribution.

In conclusion, we expect to control the acceptance systematics related to the beam geometry at a level of better than 0.1%.

Timing Difference Between Showers Induced by Positrons and Photons

A positron starts depositing energy in our calorimeter as soon as it reaches the CsI detectors. Photons from pion beta decay, on the other hand, interact initially with the detector once they are well inside it. Due to this difference the DPG is effectively shifted between the two processes. We have modeled the effect independently and in GEANT. After discovering and correcting for a "bug" in the way GEANT processes the shower particles on its stack, the results of the two methods have converged at around 80 ps. We present here the GEANT result in Fig. 14. Varying the discriminator threshold between 0.5 and 3 MeV produced a change of less than 10 ps. We believe that we can pinpoint this correction to at least 10% accuracy, or about 8 ps, which translates into a 0.03% uncertainty on the $\pi\beta$ branching ratio. We also note that the timing difference will be measured on-line and

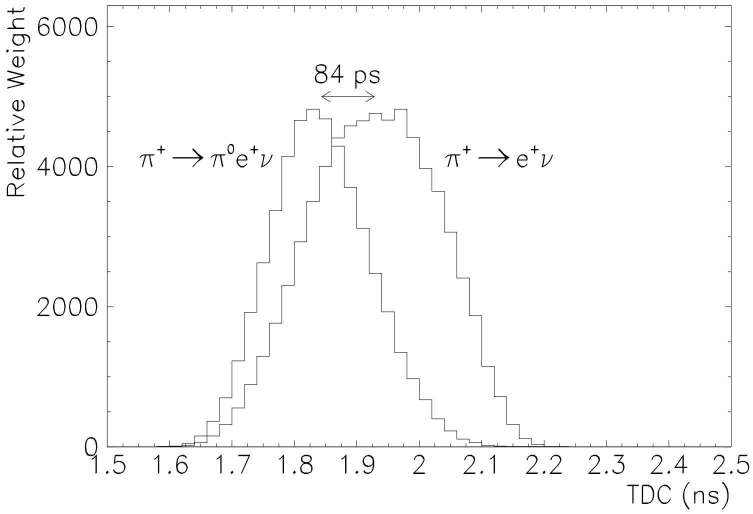

Fig. 14. TDC histograms for the $\pi^+ \rightarrow \pi^0 e^+ \nu$ and $\pi \rightarrow e\nu$ decays (GEANT simulation) for a discriminator threshold of 2 MeV.

can be evaluated from our data to test our simulations. This is true because both the $\pi\beta$ and $e\nu$ decays leave a (near) minimum ionizing positron signal in the target that can be timed against the calorimeter. With the help of the DSC digitizer and the correspondingly improved timing resolution, we should be able to verify our Monte Carlo result.

Detector Efficiences

The off-line analysis of our data will require software cuts for the suppression of unwanted background events. Among others, this will involve cuts on the charged particle counter signals. Thus the final yield will be subject to the corrections for the inefficiencies of these detectors. Inspection of Fig. 13 shows that both of the MWPC's and the plastic veto counters are positioned in such a way that their efficiencies are measured on-line throughout the experiment with very high statistics. Requiring in the offline analysis that the target, all but the detector being calibrated, and the CsI module(s) in the direct line of path of the positrons produce signals will give a robust tag, allowing for high-statistics continuous efficiency evaluation. Given prior experience in such measurements we see no reason why we should not reach uncertainty levels of the order of 10^{-4}, rendering this source of error unimportant.

Summary of Uncertainties

The uncertainties of our planned experiment fall into three categories, systematic, statistical, and errors on quantities not measured in our experiment. They are all listed below in Table 3, with the respective error limits indicated.

Table 3. Summary of the main uncertainties in determining the pion beta decay rate.

Source		Uncertainties (%)	
External			
	τ_{π^+}	0.09	
	$BR_{\pi\rightarrow\gamma\gamma}$	0.03	
	$BR_{\pi\rightarrow e\nu}$	0.33	
Total External			0.35
Systematic			
	lineshape calibration	0.2	
	π-stop geom./alignment	0.1	
	gain drift correction	<0.1	
	$\pi\beta$–$e\nu$ timing diff.	0.03	
Total Systematic			0.25
Statistical ($10^5 \pi\beta$ events)		0.32	
Overall error			0.53

4. The Collaboration

The PIBETA experiment is an international collaboration of researchers from 7 groups (UVa, PSI/Univ. of Zürich, Arizona State Univ., Swierk, Dubna, Tbilisi State Univ., and R. Bošković Inst.) Each group has the responsibility for one or more key parts of the apparatus. Equipment funding has been secured in roughly equal parts from Swiss and U.S. sources, with a considerable East European contribution in kind. These funds are, for the most part, committed or already spent.

The question of manpower for this experiment has been a longstanding concern. While all tasks are presently assigned, the experiment would greatly benefit from a strengthening of the collaboration, given the large volume of work ahead of us. The approximate current manpower commitments from the various groups are (in real time, excluding teaching or administrative duties):

UVa:	6 man-yrs/yr,
PSI:	4 man-yrs/yr,
ASU:	1 man-yr/yr,
Dubna:	2 man-yrs/yr,
Tbilisi:	1 man-yr/yr,
total:	14 man-yrs/yr.

5. The Timetable

Due to difficulties experienced by the suppliers of pure CsI modules, we have been delayed with respect to our original plans. The extra time was used for improvements in detectors, readout linearity, trigger electronics, data acquisition, DSC digitizer development, etc. Particularly beneficial was our development work on CsI detector surface treatment coupled to the 3-dimensional cosmic muon tomography technique developed specifically for this purpose, resulting in improved detector energy resolution, consistently over a large sample of modules. All these actions will eventually lead to shorter final commissioning time of the apparatus and will serve to improve the quality of our data and expedite "production" measurements.

Current timetable for the experiment is as follows:

1996: all major detector components, all of the support structure elements and control systems delivered and in place at PSI, all CsI crystals delivered, tomographed and ready for installations by the mid-year; assembly of apparatus in the fall;

1997: apparatus fully assembled at the beginning of the year; proceed with detector shakedown and calibration; begin $\pi\beta$ measurements at low pion stop rate;

1998: ramp up to the nominal operating pion stop rate ($\sim 10^6$ s^{-1}); "production" runs;

1999: more "production" runs, likely into 2000

References

1. The PIBETA home page is at URL: *http://pibeta.psi.ch* (Europe), or *http://helena.phys.-virginia.edu/~pibeta* (America).

2. J. Ahrens et al., Nucl. Phys. **A251** (1975) 478; A. Lepretre et al., Nucl. Phys. **A367** (1981) 237; H. Hebach, A. Wortberg, and M. Gari, Nucl. Phys.**A267** (1076) 425; B. L. Berman et al., Phys. Rev. **177** (1969) 1745; R. L. Bramblett et al., Phys. Rev. **148** (1966) 1198; G. G. Jonsson and B. Forkman, Nucl. Phys. **A107** (1968) 52.